Real-space observation of vibrational strong coupling between propagating phonon polaritons and organic molecules

Andrei Bylinkin[1,2], Martin Schnell[1], Marta Autore[1], Francesco Calavalle[1], Peining Li[1,3], Javier Taboada-Gutièrrez[4,5], Song Liu[6], James H. Edgar[6], Fèlix Casanova[1], Luis E Hueso[1], Pablo Alonso-Gonzalez[4,5], Alexey Y Nikitin[2,8], and Rainer Hillendrand*[7,8]

1 CIC nanoGUNE BRTA, 20018 Donostia - San Sebastian, Spain
2 Donostia International Physics Center (DIPC), 20018 Donostia-San Sebastián, Spain
3 Wuhan National Laboratory for Optoelectronics & School of Optical and Electronic Information, Huazhong University of Science and Technology, Wuhan 430074, China.
4 Departamento de Fisica, Universidad de Oviedo, 33006 Oviedo, Spain
5 Nanomaterials and Nanotechnology Research Center (CINN), El Entego, Spain
6 Tim Taylor Department of Chemical Engineering, Kansas State University Manhattan, KS 66506, USA
7 CIC nanoGUNE BRTA and EHU/UPV, 20018 Donostia-San Sebastián, Spain
8 IKERBASQUE, Basque Foundation for Science, 45011 Bilbao, Spain

Abstract

Phonon polaritons (PPs) in van der Waals (vdW) materials can strongly enhance light-matter interactions at mid-infrared frequencies, owing to their extreme infrared field confinement and long lifetimes. PPs thus bear potential for achieving vibrational strong coupling (VSC) with molecules. Although the onset of VSC has recently been observed spectroscopically with PP nanoresonators, no experiments so far have resolved VSC in real space and with propagating modes in unstructured layers. Here, we demonstrate by real-space nanoimaging that VSC can be achieved between propagating PPs in thin vdW crystals (specifically h-BN) and molecular vibrations in adjacent thin molecular layers. To that end, we performed near-field polariton interferometry, showing that VSC leads to the formation of a propagating hybrid mode with a pronounced anti-crossing region in its dispersion, in which propagation with negative group velocity is found. Numerical calculations predict VSC for nanometer-thin molecular layers and PPs in few-layer vdW materials, which could make propagating PPs a promising platform for ultra-sensitive on-chip spectroscopy and strong coupling experiments.

Main text

Phonon polaritons (PPs) – light coupled to lattice vibrations – in van der Waals (vdW) crystals open up new possibilities for infrared nanophotonics, owing to their strong infrared field confinement, picosecond-long lifetimes[1–7] and tunability via thickness and dielectric environment[8–11]. Since PPs in many vdW materials spectrally coincide with molecular vibrational resonances, which abound the mid-infrared spectral range, PP are thus promising candidates for achieving vibrational strong coupling (VSC) for developing ultrasensitive infrared spectroscopy and modification of chemical reactions by altering the vibrational energy of molecules[12–16]. Indeed, analogously to molecular vibrational infrared spectroscopy employing plasmons in graphene nanoribbons[17], localized PPs in hexagonal boron nitride (h-BN) high-Q factor nanoresonators were recently coupled to molecular vibrations[18], allowing for ultra-sensitive far-field spectroscopy at the strong coupling limit. However, ultra-confined propagating PPs in unstructured layers have neither experimentally nor theoretically been explored for field-enhanced molecular vibrational

spectroscopy or strong coupling experiments. More generally, none of the ultra-confined propagating polaritons in a 2D material has been exploited so far experimentally for field-enhanced molecular vibrational spectroscopy, although theoretical studies predict intriguing on-chip spectroscopy applications[19]. Further, real-space nanoimaging of the hybrid modes has been elusive, although it is of fundamental importance for in-depth experimental analysis of VSC exploiting PPs.

Here, we perform mid-infrared nanoimaging experiments[3–7] as a test bench to study the interaction of ultra-confined propagating polaritons in vdW materials with molecular vibrations in sub-100 nm thick organic layers. Specifically, we perform phonon-polariton interferometry of PPs in thin continuous h-BN layers interacting with 4,4′-Bis(N-carbazolyl)-1,1′-biphenyl (CPB) molecules. In contrast to typical strong coupling experiments, such as far-field spectroscopy in Kretschmann-Raether configuration or of polariton nanoresonators, we monitor in real space the effect of molecular absorption on PPs, leading to dramatic modification of the PP propagation length and anomalous dispersion with negative group velocity. We retrieve - in good agreement - experimentally and theoretically the quasi-normal modes of the CBP-PP coupled system, revealing significant anti-crossing and mode splitting caused by strong coupling. A numerical study predicts that few-layer h-BN films may enable to reach strong coupling even in the case of atomically thin molecular layers, thus underlining the potential of PPs to become a platform for ultra-sensitive on-chip spectroscopy devices.
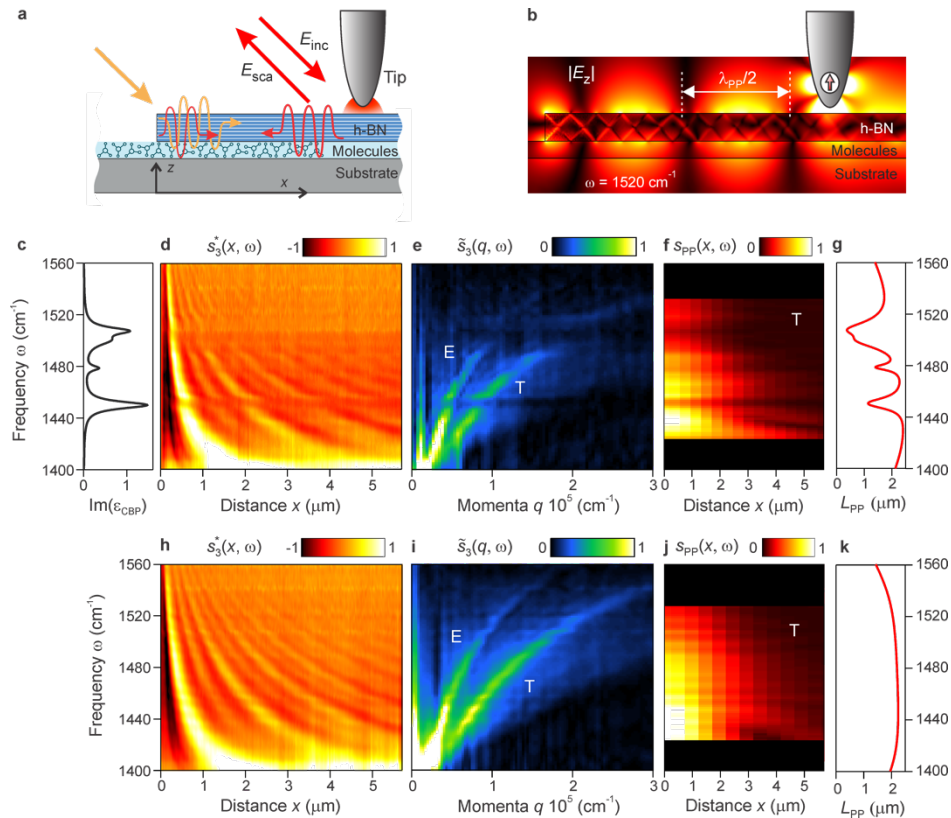
In Fig. 1a we illustrate the polariton interferometry experiment. We illuminate the metallic tip of a scattering-type scanning near-field optical microscope (s-SNOM) to launch PP modes in a thin hexagonal boron nitride (h-BN) layer, which is placed above a thin layer of CBP molecules. The tip-launched PPs propagate to the h-BN edge, reflect and propagate back to the tip. The resulting polariton interference is shown in Fig. 1b by a numerical simulation of the electric field distribution along the h-BN/CBP layer. Importantly, the PP field penetrates into the molecular layer allowing for significant interaction between PPs and molecular vibrations. By mapping and analyzing the polariton interference spectroscopically, we can study how the molecule-PP interaction modifies the polariton wavelength λ_{PP} and propagation length L_{PP}.

In a first experiment, we recorded the tip-scattered field E_{sca} (which is governed by the polariton interference) as a function of frequency ω (using the nano-FTIR spectroscopy technique, see Methods) and distance x between tip and h-BN edge (Fig. 1d). We observe the typical signal oscillations (fringes) arising from the polariton interference, whose period $\lambda_{PP}/2$ decreases with frequency ω[6]. Importantly, our data reveal interruptions of the fringes (significant reduction of the amplitude signals) at the frequencies of the molecular vibrational resonances, which are absent in the data obtained on h-BN layers without molecules (Fig. 1h), clearly indicating significant interaction between PPs and molecular vibrations.

To visualize the PP dispersion, we performed a Fourier transform (FT) of the polariton interference pattern along the x-axis, revealing two bright branches in the momentum-frequency, q-ω, domain (Fig. 1e and i for h-BN/CPB and pure h-BN layer, respectively, see Supplementary Information SII for data processing details). As in previous experiments[20], the lower momenta branch (labeled E) can be attributed to the fundamental HP slab mode (typically referred as to M0 mode) launched by the h-BN edge (Supplementary Figure S4). The higher-momenta branch (labeled T) stems from the tip-launched M0 mode, as it propagates twice the distance x. We clearly see interruptions at

the spectral position of the molecular vibrations, manifesting strong damping of the PPs by molecular absorption.

The significant interaction between molecular vibrations and PPs could lead to highly-sensitive and ultra-compact IR spectroscopy devices. To briefly discuss this interesting aspect, we isolate the near-field signal of the tip-launched mode, $s_{PP}(x,\omega)$, by filtering and directly reveal PP attenuation for each frequency ω (Fig. 1f, see Supplementary Information SII for data processing details). We observe that the PPs are less strongly excited and decay faster near the molecular vibrational resonances, demonstrating the possibility of detecting molecular vibrational signatures via the accumulated PP losses. The numerically calculated propagation lengths of the M0 mode in the presence and absence of the CPB layer (red curves in Figs. 1g,k, respectively) corroborate our experimental results qualitatively. We find a reduced propagation length at the CBP absorption bands (e.g. 0.5 μm at 1510 cm⁻¹) compared to about 2 μm on pure h-BN.

Figure 1. Phonon-polariton interferometry of molecular vibrations a, Illustration of the nanoimaging experiment. **b**, Simulated near-field distribution (z-component), generated by a point dipole source (red arrow) mimicking the illuminated tip. **c**, Imaginary part of the dielectric function ε_{cbp} of CBP molecules **d, h**, Baseline-subtracted nano-FTIR amplitude signal $s_3^*(x,\omega)$ as a function of tip-edge distance x for h-BN/CBP and pure h-BN layer. **e, i**, Amplitude of the Fourier transform of panel **d, h** along the x-axis. E and T mark the M0 mode excited by flake edge or tip, respectively. **f, j**, Isolated tip-scattered field of the M0 mode, obtained by inverse FT of the filtered T branches (Supplementary Information SII). **g, k** Theoretical propagation length L_{PP} of the M0 mode. **b-g**, h-BN thickness is 50 nm, CPB thickness is 40 nm and substrate is 150 nm SiO₂ on Si. **h-k** h-BN thickness is 50 nm and substrate is 150 nm SiO₂ on Si.
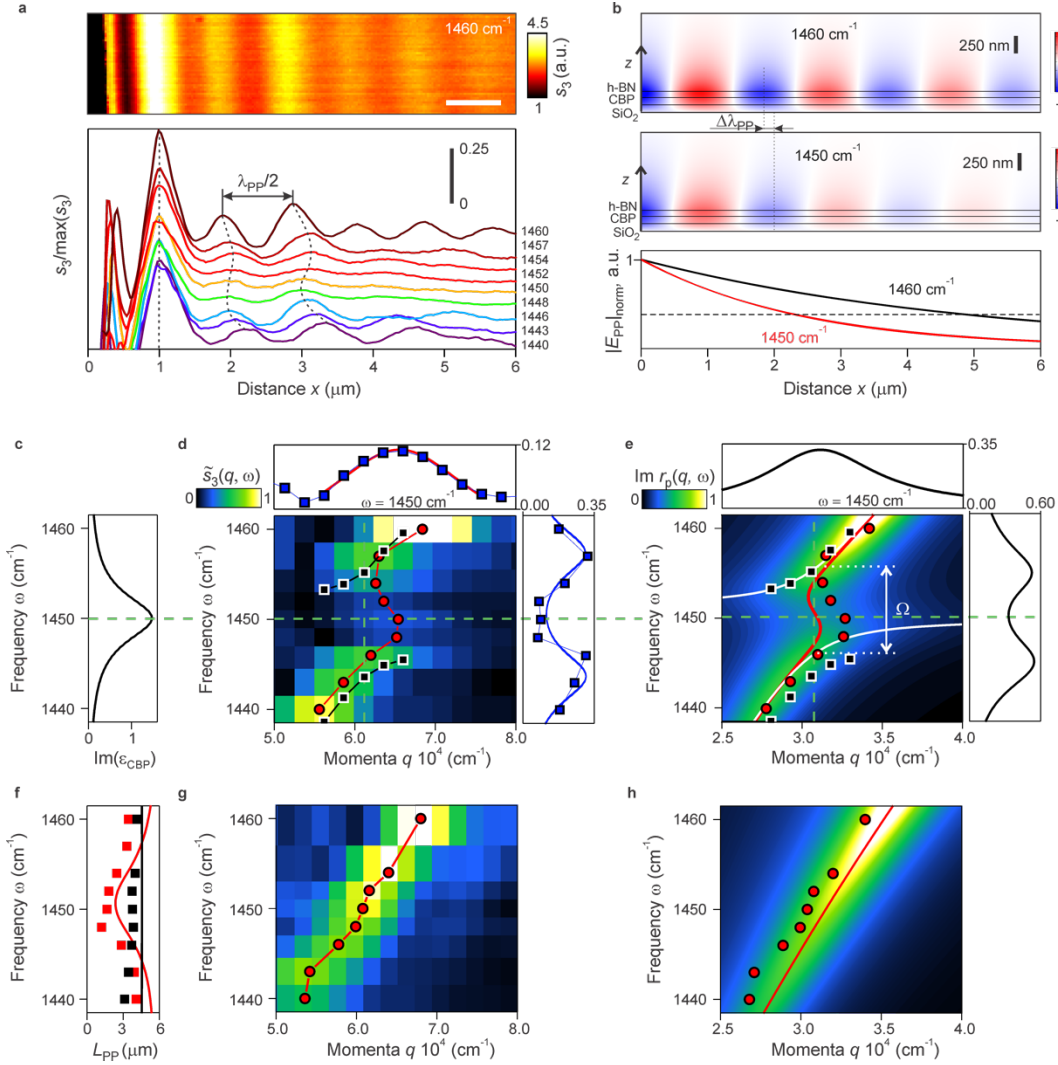
Figure 2. Real space imaging of PPs on a h-BN/CPB layer in the region of anomalous dispersion.
a, (top panel) Infrared near-field amplitude image of a 85-nm-thick h-BN flake above a 100-nm-thick CBP layer at 1460 cm^{-1}. (bottom panel) Normalized amplitude profile perpendicular to the edge at different frequencies, extracted from images such as the one shown in the top panel. **b,** (top panels) Simulated near-field distribution (z-component) of PP mode propagating along the h-BN/CPB layer. (bottom panel) Calculated absolute value of the PP field as function of propagation distance x. **c,** Imaginary part of the dielectric function ε_{CBP} of CBP molecules. **d,** Color-plot shows the amplitude of the FT of the line profiles of Fig. 2a. **e,** Color-plot $\tilde{s}_3(q, \omega)$ shows calculated imaginary part of Fresnel reflection coefficient. Curves inside color plot show calculate dispersions assuming complex-valued momentum (red) or complex-valued frequency (white). White arrow indicates mode splitting Ω. **d,e,** Blue symbols and black curves in the right and top panels show line profiles along the dashed vertical and horizontal lines, respectively. **d,** (top panel) red curve and (right panel) blue line show the Lorentz and coupled oscillators fit, respectively. **f,** Experimental (symbols) and calculated (lines) propagation length L_{PP} of PPs on h-BN/CPB (red) and pure h-BN (black) layer. **g,h,** Analogous to **d,e,** for h-BN layer without CPB.

To quantify the coupling between molecule vibrations and PPs, we performed a second experiment with improved signal-to-noise ratio and spectral resolution. To that end, we imaged PPs on a 85 nm thick h-BN layer above a 100 nm thick CPB layer at various frequencies around the CPB

4

vibration at 1450 cm^{-1} employing a quantum cascade laser (QCL) (Fig. 2a, top; see Methods). From the images we extracted line profiles (Fig. 2a, bottom; see Methods), which let us immediately recognize anomalous dispersion[21–24], near the CBP resonance. We clearly see that the PP wavelength λ_{PP} increases as the molecular resonance is crossed from 1446 to 1454 cm^{-1} (indicated by black dashed lines in Fig. 2a). To analyze the corresponding dispersion, we assembled FTs of the line profiles into a $\tilde{s}_3(q,\omega)$ plot (Fig. 2d, see Supplementary Information SIII for data processing details). By fitting the $\tilde{s}_3(q,\omega)$ in q-direction using Lorentz function and marking the maxima (red symbols in Fig. 2d), we clearly see that molecular absorption introduces a back bending in the PP dispersion, in stark contrast to the PP dispersion observed for h-BN without molecules (Fig. 2g, obtained analogously to Fig. 2d for pure h-BN layer). Further, the propagation length is significantly reduced by the presence of molecules (red symbols in Fig. 2f). Both observations represent a fundamental landmark feature of strong interaction between a propagating mode and a dipolar excitation, here, for the first time, observed in real space for ultra-confined phonon polaritons coupled to molecular vibrations. The near-field simulation shown in Fig. 2b confirms the reduction of both wavelength and propagation length when frequency decreases from 1460 to 1450 cm^{-1}.

The significant back bending of the dispersion indicates strong coupling between the PPs and the molecular vibrations of CPB, which in the following we corroborate by quasi-normal mode analysis. To this end, we extracted $\tilde{s}_3(\omega)$ line profiles from Fig. 2d for fixed momenta q and fitted the data with a coupled-oscillator model[18,25,26] (see Supplementary Information SIV), yielding the dispersion of the quasi-normal modes, $\omega_{\pm}(q)$ (black symbols in Fig. 2d)[27]. The right panel of Fig. 2d shows, exemplarily, the experimental line profile (blue symbols) and coupled oscillator fit (blue line) for the q-value marked by the vertical dashed line in the $\tilde{s}_3(q,\omega)$-plot. We observe a clear anti-crossing behavior of the quasi-normal modes at the CBP resonance and a mode splitting of Ω = 11 cm^{-1}. Considering the uncoupled PP and CPB linewidths of $\Gamma_{PP} = 8$ cm^{-1} and $\Gamma_{CBP} = 6.4$ cm^{-1}, respectively (Methods), we find that the strong coupling condition $C \equiv \dfrac{\Omega^2}{\left(\dfrac{\Gamma_{CBP}^2}{2} + \dfrac{\Gamma_{PP}^2}{2}\right)} =$

2.3 > 1 is well fulfilled[28].

To interpret the $\tilde{s}_3(q,\omega)$ data and to verify the extracted experimental dispersions, we performed a theoretical eigenmode analysis. To that end, we calculated the Fresnel reflection coefficient, r_p, of h-BN/CPB and pure h-BN layers on the SiO$_2$/Si substrate employing the transfer matrix (TM) method[29] (see Methods). We find that the Im(r_p) plotted as a function of real q and ω (Fig. 2e,h) describes well the experimental data $\tilde{s}_3(q,\omega)$ (Fig. 2d,g), particularly peak positions, linewidths and the saddle point at the CPB resonance, demonstrating that spatially Fourier transformed spectral polariton interferometry can be interpreted analogously to momentum- and frequency-resolved surface plasmon resonance spectroscopy employing, for example, the classical Kretschmann-Raether configuration[28,30–33].

To obtain the eigenmode dispersions, we determined the poles of r_p, assuming either complex momenta $q + i\kappa$ (corresponding to spatially decaying modes with propagation length $L_{PP} = 1/\kappa$) or complex frequencies $\omega - i\gamma$ (corresponding to temporally decaying modes with lifetime $\tau = 1/\gamma$). For spatially decaying modes in h-BN/CPB layers, we find a continuous dispersion exhibiting back bending (compare red curve in Fig. 2e with red curve in Fig. 2h showing results for pure h-BN layer) and reduced propagation lengths L_{PP} around the CPB resonance (compare red curve in Fig.

2f with black curve showing L_{PP} for pure h-BN layer). In contrast, analysis of temporally decaying modes yields quasi-normal modes featuring anti-crossing (white curves in Fig. 2e) and mode splitting of $\Omega = 10$ cm^{-1}, which according to C = 1.9 indicates strong coupling. The excellent agreement between experimental dispersions and propagation lengths (solid lines vs. symbols in Figs. 2e,f) clearly demonstrates the unique capability of polariton interferometry for comprehensive and quantitative analysis of the coupling between ultra-confined propagating polaritons and dipolar excitations, here specifically revealing strong coupling between propagating phonon polaritons and molecular vibrations.

We deepen the insights into strong coupling between molecular vibrations and PPs by an eigenmode analysis via TM calculations (analog to Fig. 2e) for various h-BN and CPB layer thicknesses. We first consider a variation of the CPB layer thickness d_{CPB} for a fixed h-BN thickness of 35 nm (Fig. 3b-f). We find that the region of anomalous dispersion widens when d_{CPB} is increased, which comes along with a reduction of the PP propagation length L_{PP} (i.e. increase of PP damping) that reaches a finite minimum at the molecular resonance (Fig. 3c). Further, we find that with increasing d_{CPB} the mode splitting Ω (the smallest vertical separation between the real frequency of the quasi-normal modes) and thus the coupling strength between PPs and molecular vibrations increases (Fig. 3e), as simply more of the PP fields lies inside the CBP layer (illustrated in Fig. 3(a)). Interestingly, the life times are rather large, about 2 ps, for all considered d_{CPB} (red curves in Fig. 3f, obtained from the eigenmode analysis describe above), which is close to the molecular resonance lifetime of 1.7 ps and emphasizes that the coupled mode becomes more determined by the character of molecular absorption near the resonance. Note that in the region of anomalous dispersion PPs propagate with negative group velocity, $v_g = d\omega/dq < 0$ (Fig. 2d and Fig. 3b), yet with finite propagation length (red symbols in Fig. 2f and Fig. 3c). A simulation of the decay of narrowband PP pulses illustrates this effect (Fig. 3d). In the presence of a molecular layer, we find that the maximum of the pulse envelope after propagation of $x = 1.5$ μm appears at negative times t. Importantly, the negative group velocity yields negative values for the life time τ when calculated according to $\tau = L_{PP}/v_g$ (black curves in Fig. 3f), implying that this lifetime determination – typically applied in polariton interferometry[3,4,34] – cannot be used in the case of anomalous dispersion. Instead, eigenmode analysis in the picture of a temporally decaying mode is required (red curves in Fig. 3f).
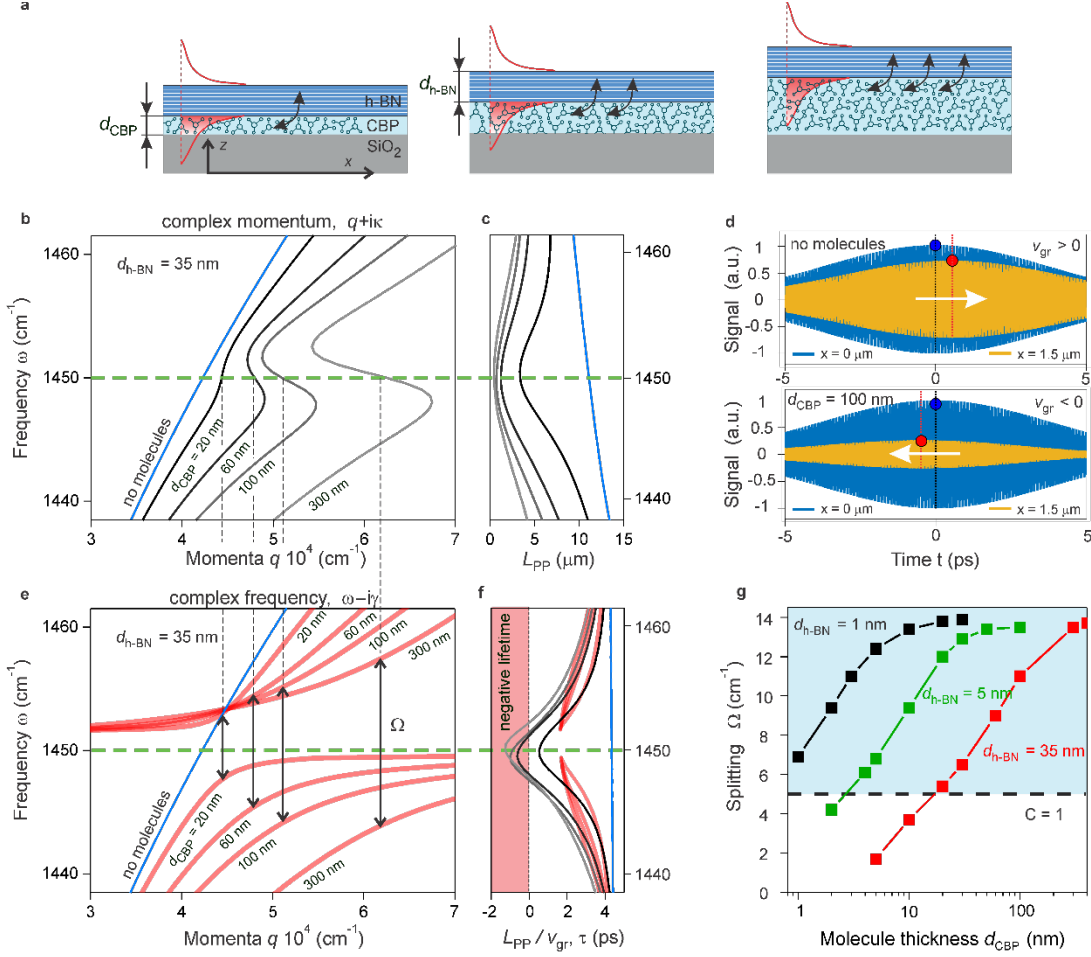
Figure 3. Dispersion and mode splitting. a, Illustration of phonon polaritons on differently thick molecular layers. **b,e,** Dispersions of PPs in a 35 nm-thick h-BN layer on CPB layers of various thicknesses d_{CBP}, obtained by eigenmode analysis via TM calculations assuming complex wavevectors $q + i\kappa$ (panel **b**) or complex frequencies $\omega - i\gamma$ (panel **e**). Horizontal green dashed line marks the frequency of the molecular vibrational resonance. **c**, PP propagation length. **d,** Narrowband PP pulses with 1450 cm⁻¹ center frequency and 3.5 cm⁻¹ spectral width at positions x = 0 and x = 1.5 μm in absence (top panel) and presence (bottom panel) of 100 nm-thick CBP layer below a 35 nm-thick h-BN layer. **f,** Blue and red lines show PP lifetime according to $\tau = 1/\gamma$. Black and gray lines show L_{PP}/v_{gr}. **g,** Mode splitting Ω as a function of the molecular layer thickness d_{CBP} for h-BN layer with thickness $d_{h\text{-}BN}$ of 1 nm (black squares), 5 nm (green squares) and 35 nm (red squares). Horizontal black dashed line indicates the strong-coupling limit.

Plotting Ω as a function of d_{CBP} (red symbols in Fig. 3g), we find saturation at about 14 cm⁻¹ for $d_{CBP} > 300$ nm, where the whole PP lies inside the CPB layer. Considering that the condition C > 1 in our simulations is fulfilled for $\Omega > 5$ cm⁻¹ (Supplementary Info SV, we find that strong coupling of CPB vibrations and PPs in a 35 nm tick h-BN layer can be already achieved for d_{CPB} > 20 nm. Remarkably, further numerical mode analysis for h-BN layers with reduced thickness of $d_{h\text{-}BN} = 5$ nm and 1 nm (green and black symbols in Fig. 3g, respectively) predicts that in future experiments strong coupling may be achieved, remarkably, with few CPB monolayers ($d_{CPB} < 2$

nm). This can be explained by the extreme mode compression that comes along with the 100-fold reduced PP wavelength compared to the photon wavelength of the same energy[35].

Our work demonstrates that propagating PP in unstructured vdW materials can strongly couple to molecular vibrations, which could provide a platform for testing strong coupling and local controlling of chemical reactivity[12–15]. In addition, it opens up possibility for ultracompact, on-chip spectroscopy[19]. A large variety of vdW materials are at the disposal to go beyond the spectral range of h-BN, as recently demonstrated by PP observation on MoO_3[4] and V_2O_5[34]. In contrast to conventional polaritonic spectroscopy made with resonators (as, e.g. ribbons[18], cones[36] or hole arrays[37]) our work opens new avenues for studying strong-light matter interactions without the need of challenging sample structuring that typically comes along with additional losses from sample damage, inhomogeneities and scattering due to uncertainties in the sample fabrication process.

Acknowledgements

Competing interests

R.H. is co-founder of Neaspec GmbH, a company producing scattering-type scanning near-field optical microscope systems, such as the one used in this study. The remaining authors declare no competing interests.

References

1. Basov, D. N., Fogler, M. M. & García De Abajo, F. J. Polaritons in van der Waals materials. *Science (80-.).* **354**, aag1992 (2016).

2. Low, T. *et al.* Polaritons in layered two-dimensional materials. *Nat. Mater.* **16**, 182–194 (2017).

3. Giles, A. J. *et al.* Ultralow-loss polaritons in isotopically pure boron nitride. *Nat. Mater.* **17**, 134–139 (2018).

4. Ma, W. *et al.* In-plane anisotropic and ultra-low-loss polaritons in a natural van der Waals crystal. *Nature* **562**, 557–562 (2018).

5. Zheng, Z. *et al.* Highly Confined and Tunable Hyperbolic Phonon Polaritons in Van Der Waals Semiconducting Transition Metal Oxides. *Adv. Mater.* **30**, (2018).

6. Dai, S. *et al.* Tunable phonon polaritons in atomically thin van der Waals crystals of boron nitride. *Science (80-.).* **343**, 1125–1129 (2014).

7. Yoxall, E. *et al.* Direct observation of ultraslow hyperbolic polariton propagation with

negative phase velocity. *Nat. Photonics* **9**, 674–678 (2015).

8.   Dai, S. *et al.* Graphene on hexagonal boron nitride as a tunable hyperbolic metamaterial. *Nat. Nanotechnol.* **10**, 682–686 (2015).

9.   Kim, K. S. *et al.* The Effect of Adjacent Materials on the Propagation of Phonon Polaritons in Hexagonal Boron Nitride. *J. Phys. Chem. Lett.* **8**, 2902–2908 (2017).

10.   Fali, A. *et al.* Refractive Index-Based Control of Hyperbolic Phonon-Polariton Propagation. *Nano Lett.* **19**, 7725–7734 (2019).

11.   Dai, S. *et al.* Hyperbolic Phonon Polaritons in Suspended Hexagonal Boron Nitride. *Nano Lett.* **19**, 1009–1014 (2019).

12.   Thomas, A. *et al.* Tilting a ground-state reactivity landscape by vibrational strong coupling. *Science (80-.).* **363**, 615–619 (2019).

13.   Herrera, F. & Owrutsky, J. Molecular polaritons for controlling chemistry with quantum optics. *J. Chem. Phys.* **152**, (2020).

14.   Thomas, A. *et al.* Ground-State Chemical Reactivity under Vibrational Coupling to the Vacuum Electromagnetic Field. *Angew. Chemie* **128**, 11634–11638 (2016).

15.   Ribeiro, R. F., Martínez-Martínez, L. A., Du, M., Campos-Gonzalez-Angulo, J. & Yuen-Zhou, J. Polariton chemistry: controlling molecular dynamics with optical cavities. *Chem. Sci.* **9**, 6325–6339 (2018).

16.   Feist, J., Galego, J. & Garcia-Vidal, F. J. Polaritonic Chemistry with Organic Molecules. *ACS Photonics* **5**, 205–216 (2018).

17.   Rodrigo, D. *et al.* Mid-infrared plasmonic biosensing with graphene. *Science (80-.).* **349**, 165–168 (2015).

18.   Autore, M. *et al.* Boron nitride nanoresonators for Phonon-Enhanced molecular vibrational spectroscopy at the strong coupling limit. *Light Sci. Appl.* **7**, 17172–17178 (2018).

19.   Francescato, Y., Giannini, V., Yang, J., Huang, M. & Maier, S. A. Graphene Sandwiches as a Platform for Broadband Molecular Spectroscopy. *ACS Photonics* **1**, 437–443 (2014).

20.   Yoxall, E. *et al.* Direct observation of ultraslow hyperbolic polariton propagation with negative phase velocity. *Nat. Photonics* **9**, 674–678 (2015).

21.   Hu, F. *et al.* Imaging exciton-polariton transport in MoSe 2 waveguides. *Nat. Photonics* **11**, 356–360 (2017).

22.   Arakawa, E. T., Williams, M. W., Hamm, R. N. & Ritchie, R. H. Effect of Damping on Surface Plasmon Dispersion. *Phys. Rev. Lett.* **31**, 1127–1129 (1973).

23.   Pockrand, I. & Swalen, J. D. Anomalous Dispersion of Surface Plasma Oscillations. *J Opt Soc Am* **68**, 1147–1151 (1978).

24.   Schuller, E. & Falge, H. J. Dispersion curves of surface phonon-polaritons with backbending. **54**, 317–318 (1975).

25.   Novotny, L. Strong coupling, energy splitting, and level crossings: A classical perspective. *Am. J. Phys.* **78**, 1199–1202 (2010).

26.   Wu, X., Gray, S. K. & Pelton, M. Quantum-dot-induced transparency in a nanoscale plasmonic resonator. *Opt. Express* **18**, 23633 (2010).

27.   Hennessy, K. *et al.* Quantum nature of a strongly coupled single quantum dot-cavity system. *Nature* **445**, 896–899 (2007).

28.   Törmö, P. & Barnes, W. L. Strong coupling between surface plasmon polaritons and emitters: A review. *Reports Prog. Phys.* **78**, 13901 (2015).

29.   Passler, N. C. & Paarmann, A. Generalized 4 × 4 matrix formalism for light propagation in anisotropic stratified media: study of surface phonon polaritons in polar dielectric heterostructures. *J. Opt. Soc. Am. B* **34**, 2128 (2017).

30.   Pockrand, I., Brillante, A. & Möbius, D. Exciton-surface plasmon coupling: An experimental investigation. *J. Chem. Phys.* **77**, 6289–6295 (1982).

31.   Bellessa, J., Bonnand, C., Plenet, J. C. & Mugnier, J. Strong coupling between surface plasmons and excitons in an organic semiconductor. *Phys. Rev. Lett.* **93**, 036404–1 (2004).

32.   Memmi, H., Benson, O., Sadofev, S. & Kalusniak, S. Strong Coupling between Surface Plasmon Polaritons and Molecular Vibrations. *Phys. Rev. Lett.* **118**, 1–5 (2017).

33.   Shlesinger, I. *et al.* Strong Coupling of Nanoplatelets and Surface Plasmons on a Gold Surface. *ACS Photonics* **6**, 2643–2648 (2019).

34.   Taboada-Gutiérrez, J. *et al.* Broad spectral tuning of ultra-low-loss polaritons in a van der Waals crystal by intercalation. *Nat. Mater.* 0–5 (2020) doi:10.1038/s41563-020-0665-0.

35.   Dai, S. *et al.* Phonon Polaritons in Monolayers of Hexagonal Boron Nitride. *Adv. Mater.* **31**, 1–5 (2019).

36.   Caldwell, J. D. *et al.* Sub-diffractional volume-confined polaritons in the natural hyperbolic material hexagonal boron nitride. *Nat. Commun.* **5**, 1–9 (2014).

37.   Alfaro-Mozaz, F. J. *et al.* Deeply subwavelength phonon-polaritonic crystal made of a van der Waals material. *Nat. Commun.* **10**, 1–7 (2019).

38.   Liu, S. *et al.* Single Crystal Growth of Millimeter-Sized Monoisotopic Hexagonal Boron Nitride. *Chem. Mater.* **30**, 6222–6225 (2018).

Methods

Sample preparation

4,4′-bis(N-carbazolyl)-1,1′-biphenyl with sublimed quality (99.9%) (Sigma-Aldrich, Saint Louis, MO, USA) was thermally evaporated in an ultra-high vacuum evaporator chamber (base pressure <10^{-9} mbar), at a rate of 0.1 nm s^{-1} using a Knudsen cell.

The h-BN crystal flake was grown from a metal flux at atmospheric pressure as described previously[38]. The thin layers used in this study were prepared by mechanical exfoliation with blue Nitto tape. Then we performed a second exfoliation of the h-BN flakes from the tape onto a transparent polydimethylsiloxane stamp. Using optical inspection of the h-BN flakes on the stamp,

we identified high-quality flakes with appropriate thickness. These flakes were transferred onto a Si/SiO2/CBP substrate using the deterministic dry transfer technique.

Nanoscale Fourier transform infrared spectroscopy

We used nanoscale Fourier transform infrared (nano-FTIR) spectroscopy to perform phonon-polariton interferometry of molecular vibrations experiment. We used a commercial scattering-type scanning near-field optical microscope setup equipped with a nano-FTIR module (Neaspec GmbH, Martinsried, Germany), in which the oscillating (at a frequency $\Omega \cong 270$ KHz) metal-coated (Pt/Ir) AFM tip (Arrow-NCPt-50, Nanoworld, Nano-World AG, Neuchâtel, Switzerland) is illuminated by p-polarized mid-IR broadband radiation generated by a supercontinuum laser (Femtofiber pro IR and SCIR; Toptica, Gräfelfing, Germany; average power of about 0.5mW; frequency range 1200–1700 cm^{-1}).). The spectral resolution was set to 6.25 cm^{-1}, which is the limit of the microscope. The spatial step size of the line scan was set to 20 nm per pixel for line scan with molecules Fig.1d (length was 6 μm, number of pixels was 300). The spatial step size of the line scan was set to around 27 nm per pixel for line scan without molecules Fig.1g (length was 8 μm, number of pixels was 300. To suppress background scattering from the tip shaft and sample, the detector signal was demodulated at a frequency 3Ω. The nano-FTIR spectra was normalized to the spectra of Si substrate, $s_3(x,\omega)e^{i\varphi_3(x,\omega)} = s_3^{h-BN/CBP}(x,\omega)e^{i\varphi_3^{h-BN/CBP}(x,\omega)}/s_3^{Si}(\omega)e^{i\varphi_3^{Si}(\omega)}$.

Infrared nanoimaging via sSNOM employing QCL

We used a commercial scattering-type scanning near-field optical microscope setup (Neaspec GmbH, Martinsried, Germany), in which the oscillating (at a frequency $\Omega \cong 270$ KHz) metal-coated (Pt/Ir) AFM tip (Arrow-NCPt-50, Nanoworld, Nano-World AG, Neuchâtel, Switzerland) is illuminated by p-polarized mid-IR wavelength-tunable quantum cascade laser (QCL). The backscattered light is collected with a pseudo-heterodyne interferometer. To suppress background scattering from the tip shaft and sample, the detector signal was demodulated at a frequency 3Ω

Figure 2a (top panel) shows a representative near-field amplitude, s_3, image of a 80-nm-thick hBN flake above a 100-nm-thick CBP layer at $\omega = 1460$ cm^{-1}. By imaging the same sample area at various frequencies and averaging them in direction parallel to the hBN edge, we obtained the near-field line profiles, Figure 2a (bottom panel).

Eigenmode analysis

We use the transfer matrix approach to calculate the polariton eigenmodes[29]. The eigenmodes of polaritons in a layers sample can be found as the poles in the Fresnel reflectivity of the p-polarized light r_p of the layers. In the case of the spatially decaying mode, the eigenmodes would appear considering the complex momenta, $q+i\kappa$. We determine the poles of $r_p(q+i\kappa, \omega)$ to obtain $\omega(q)$ and the propagation length $L_{pr} = 1/\kappa$, where κ is spatial damping. In case of the temporally decaying mode, the eigenmodes would appear considering the complex frequency, $\omega-i\gamma$. We determine the poles of $r_p(q, \omega-i\gamma)$ to obtain $\omega(q)$ and the lifetime $\tau = 1/\gamma$, where the γ is temporal damping and mode linewidth $\Gamma = \gamma/2$. The dielectric permittivity of h-BN, CBP, Si and SiO$_2$ were modeled as described in Supplementary Information SI.

Electromagnetic simulations

Full-wave numerical simulations using the finite-elements method in frequency domain (COMSOL) were performed to study the field distribution around the h-BN/CBP heterostructure on top of Si/SiO$_2$ substrate. The dielectric permittivity of h-BN, CBP, Si and SiO$_2$ were modeled as described in Supplementary Information SI.